Analytical and Bioanalytical Chemistry (2022) 414:1651–1662
https://doi.org/10.1007/s00216-021-03789-4

RESEARCH PAPER

Ratiometric fluorescence and colorimetric dual-mode sensing platform based on carbon dots for detecting copper(II) ions and D-penicillamine

Wei Zhang[1] · Yu Zhang[2] · Xin Liu[1] · Yue Zhang[1] · Yibing Liu[1] · Wei Wang[1] · Rui Su[1] · Ying Sun[1] · Yibing Huang[2] · Daqian Song[1] · Yanhua Wu[3] · Xinghua Wang[1]

Received: 7 May 2021 / Revised: 27 October 2021 / Accepted: 11 November 2021 / Published online: 6 January 2022

Abstract

A sensing platform with both ratiometric fluorescence and colorimetric responses towards copper(II) ions (Cu^{2+}) and D-penicillamine (D-pen) was constructed based on carbon dots (CDs). *o*-Phenylenediamine (OPD) was employed as a chromogenic development reagent for reaction with Cu^{2+} to generate the oxidation product 2,3-diaminophenazine (oxOPD), which not only emits green fluorescence at 555 nm, but also quenches the blue fluorescence of CDs at 443 nm via the inner filter effect (IFE) and Förster resonance energy transfer (FRET). Additionally, oxOPD exhibits obvious absorption at 420 nm. Since the intense chelation affinity of D-pen to Cu^{2+} greatly inhibits the oxidation of OPD, the intensity ratio of fluorescence at 443 nm to that at 555 nm (F_{443}/F_{555}) and the absorbance at 420 nm (A_{420}) were conveniently employed as spectral response signals to represent the amount of D-pen introduced into the testing system. This dual-signal sensing platform exhibits excellent selectivity and sensitivity towards both Cu^{2+} and D-pen, with low detection limits of 0.019 μM and 0.092 μM, respectively. In addition, the low cytotoxicity of the testing reagents involved in the proposed sensing platform facilitates its application for live cell imaging.

Keywords Ratiometric fluorometry · Colorimetry · D-Penicillamine · Copper ion · Carbon dots · Cell imaging

Introduction

D-penicillamine (D-pen) is a common reagent for detoxification of heavy metals in organisms. D-pen can form water-soluble complexes with metal ions due to the intense chelation affinity of sulfhydryl and amino groups towards metal ions, which aids in expelling toxic metal ions such as Cu^{2+}, Al^{3+}, Hg^{2+} and Zn^{2+} from the body [1]. D-pen can also be used to treat certain autoimmune diseases including rheumatoid arthritis, chronic active hepatitis, scleroderma, mouth/eye dryness and arthritis symptoms [2–4]. However, excessive use of D-pen can cause side effects such as cystinuria and thrombocytopenia [5]. Therefore, it is important to quantitatively determine the concentration of D-pen in human tissues or body fluids during related clinical treatments.

Copper ions (Cu^{2+}) are essential to the metabolism of living organisms and play an important role in intracorporeal biological processes, especially in cellular processes of respiration, neural transmission and defense against oxidative tissue injury or stress [6–8]. Excessive or defective copper in the human body may cause adverse effects or neurological diseases such as Menkes syndrome and Wilson's disease [9]. Thus, developing novel methods for the sensitive and rapid detection of Cu^{2+} in live cells is necessary for clinical diagnosis.

Fluorescent carbon dots (CDs), as fluorescent nanomaterials, have attracted much attention since their discovery in 2004, due to their unique optical and electronic properties [10–12]. Compared with fluorescent semiconductor quantum dots (QDs) and metal nanoclusters, CDs display conspicuous

✉ Yanhua Wu
wuyanhua@jlu.edu.cn

✉ Xinghua Wang
starred.wang@gmail.com

1 College of Chemistry, Jilin University, Qianjin Street 2699, Changchun 130012, China

2 College of Life Sciences, Jilin University, Qianjin Street 2699, Changchun 130012, China

3 Division of Clinical Research, The First Hospital of Jilin University, Changchun 130021, China

features including a facile synthetic process, low toxicity, remarkable biocompatibility and water solubility [13–16], making them a promising fluorescence indicator for bioanalysis and clinical diagnosis.

Various analytical methods have been reported for detecting D-pen in organisms, including chemiluminescence [17], fluorometry [18], spectrophotometry [19], electrochemistry [20], infrared spectrometry [21], and chromatography [22]. Although most of these methods provide adequate sensitivity for detecting D-pen, the sophisticated and time-consuming procedures for sample pretreatment and expensive testing instruments or reagents limit their applications. Fluorometry based on novel fluorescent nanomaterials such as CDs [23] and quantum dots (QDs) [24] has been widely employed in clinical diagnosis owing to its sufficient sensitivity, convenience, and rapidity, and it also possesses the potential for detecting D-pen in biological samples.

In recent years, many strategies have been established for detection of Cu^{2+}, including inductively coupled plasma mass spectrometry [25], surface-enhanced Raman scattering [26], atomic absorption spectroscopy [27], atomic emission spectroscopy [28], electrochemistry [29], fluorometry [30] and photoelectrochemical sensing technology [31]. In particular, fluorescence probes based on QDs [32] and CDs [33] have been proven effective for detecting Cu^{2+} in both aqueous and biological samples, due to the simple synthesis and the good biocompatibility of fluorescent quantum dots as well as the highly sensitive nature of fluorescence.

Ratiometric fluorometry is generally carried out by monitoring fluorescence intensities at two emission wavelengths, and then using the ratios of these intensities as response signals to reduce the noise of the testing environment and eliminate fluctuations in the fluorophotometer [34, 35]. Compared with routine fluorometry using fluorescence intensities at a single emission wavelength as response signals, ratiometric fluorometry can generally provide superior sensitivity and excellent precision for detection of the same target [36]. The key requirement for establishing a ratiometric fluorescence method is constructing a response system with two fluorescence emissions varied in opposite trends along the variations of target amount under excitation at one wavelength.

We constructed a dual-mode sensing platform (Scheme 1) with both ratiometric fluorescence and colorimetric readouts based on fluorescent CDs and o-phenylenediamine (OPD) for sensitive detection of Cu^{2+} and D-pen

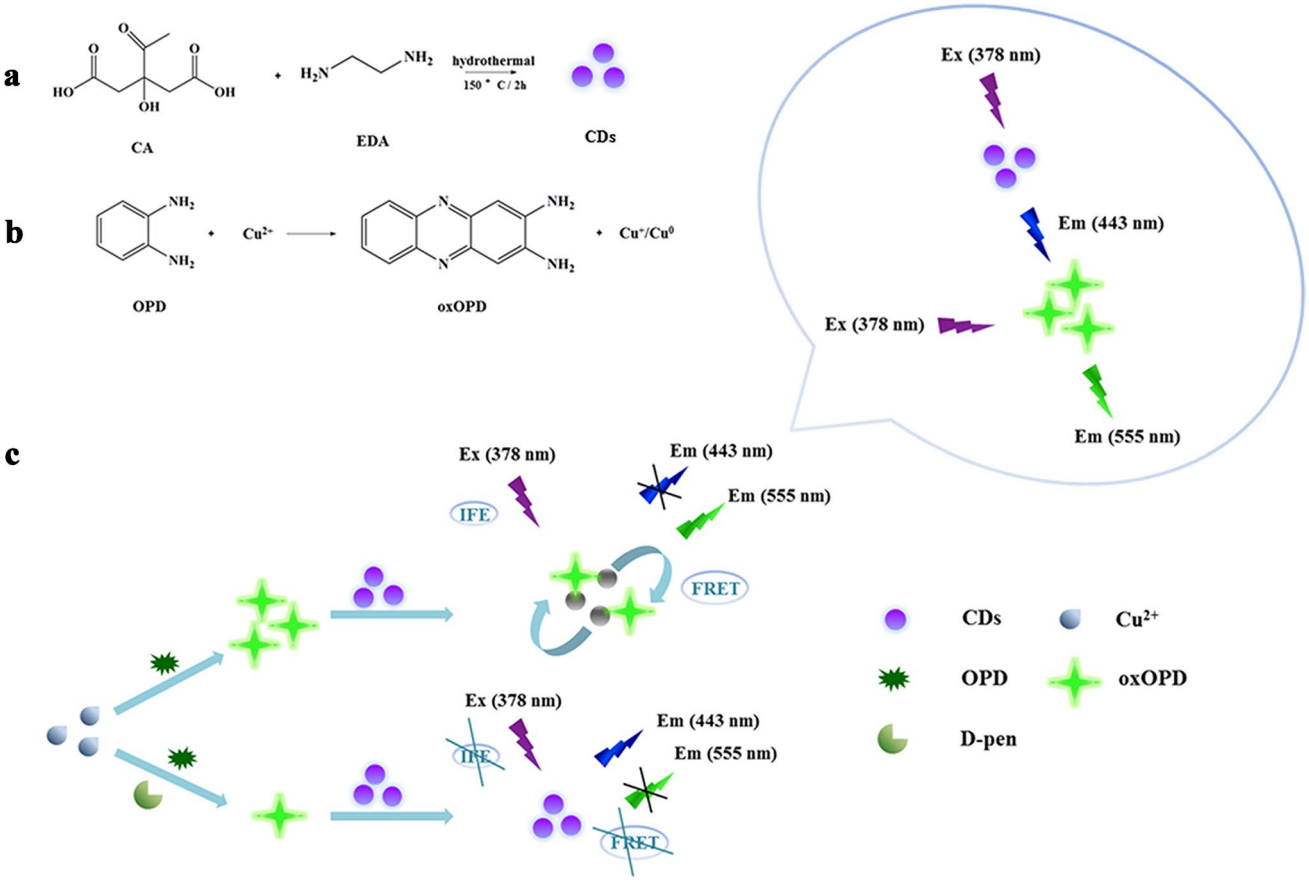

Scheme 1 Schematic diagram for detection of Cu^{2+} and D-pen.

in body fluids. In this sensing platform, OPD was oxidized to 2,3-diaminophenazine (oxOPD) by Cu^{2+} (Scheme 1b). Under excitation at 378 nm, CDs and oxOPD emitted fluorescence at 443 nm and 555 nm, respectively. The competitive absorption of excitation irradiation induced the inner filter effect (IFE) of CDs and oxOPD on each other. Moreover, the Förster resonance energy transfer (FRET) between CDs and oxOPD in the testing system occurred due to the overlap of their respective emission and absorption spectra, as well as the appropriate spatial distance between them. Both the IFE and the FRET would result in the quenching of fluorescence at 443 nm emitted from CDs, since the amount of CDs in this sensing platform was set as a constant value. Therefore, intensities of fluorescence at 443 nm and 555 nm were both determined by the amount of oxOPD in this sensing platform. After introducing D-pen into this sensing platform, the oxidation of OPD was inhibited due to the strong chelation interaction between D-pen and Cu^{2+}, resulting in both limited fluorescence quenching of CDs and constrained fluorescence emission of oxOPD, and consequently, an increase in the fluorescence intensity ratio F_{443}/F_{555} was observed. Additionally, absorption of oxOPD at 420 nm (A_{420}), which was determined by the amount of oxOPD in the testing system, provided the colorimetric readout of this sensing platform. This sensing platform was applied to detect D-pen in human serum and urine samples. Furthermore, the proposed fluorescence response mechanism towards D-pen was employed for fluorescence imaging of live cells.

Experimental

Instrumentation

Fluorescence spectra were recorded by a F-2700 fluorescence spectrophotometer (Hitachi Ltd., Japan). Ultraviolet-visible (UV-Vis) absorption spectra were collected on a Cary 60 spectrometer (Agilent Technologies Inc., USA). Morphology features of CDs were characterized by an H-8100 transmission electron microscope (TEM, Hitachi High-Tech Co., Japan) at an operating voltage of 200 kV. X-ray photoelectron spectroscopy (XPS) spectra were measured on an ESCALAB 250 spectrometer (Thermo Fisher Scientific Inc., USA). A Nicolet iS5 Fourier transform infrared (FT-IR) spectrometer (Thermo Fisher Scientific Inc., USA) was employed to identify functional groups on the surface of CDs. Fluorescence lifetime measurements were carried out on a FLS920 steady-state and transient-state fluorescence spectrometer (Edinburgh Instruments Ltd., UK). Fluorescence imaging of live cells was performed on an LSM 710 confocal microscope (Carl Zeiss Microscopy GmbH, Germany).

Reagents and samples

Tris-(hydroxymethyl)aminomethane and D-pen were purchased from Aladdin Reagent Co., Ltd., China. o-Phenylenediamine (OPD) was purchased from Energy Chemical Co., Ltd., China. All the metal salts containing nitrate, perchlorate, sulfite and thiocyanate anions were purchased from Sinopharm Chemical Reagent Co., Ltd., China. $Cu(NO_3)_2{\cdot}3H_2O$ was dehydrated for preparing standard Cu^{2+} aqueous solution. Stock aqueous solutions of other metal ions including K^+, Na^+, Ca^{2+}, Mn^{2+}, Ag^+, Fe^{3+}, and Hg^{2+} were prepared from their perchlorate salts. Inorganic anions including SO_3^{2-} and SCN^- were prepared using their sodium salts. Biological substances including ascorbic acid (AA), uric acid (UA), bovine serum albumin (BSA), glucose (Glu), α-lactose (α-Lac), lactose (Lac), tyrosine (Tyr), phenprobamate (Phe), valine (Val), histidine (His), arginine (Arg), threonine (Thr), L-methionine (Met), L-lysine (Lys) and tryptophan (Trp) were purchased from Shanghai Yuanye Bio-Technology Co., Ltd., China. All chemical reagents were of analytical grade and were used as received without further purification. Ultrapure water with resistivity of 18.2 MΩ-cm was prepared using a GBW purification system (Beijing Purkinje General Instrument Co, China). Three human serum samples and three human urine samples from six individual healthy volunteers were provided by the First Hospital of Jilin University (Changchun, China). It was confirmed that none of the volunteers had ever taken or been injected with D-pen. The A549 lung cancer cells used in this work were purchased from Procell Life Science & Technology Co., Ltd., (Wuhan, China).

Synthesis of fluorescent CDs

The CDs were synthesized according to a reported hydrothermal method [37]. Briefly, 0.5 g of citric acid and 0.25 mL of ethylenediamine were dissolved in 10 mL of ultrapure water. Then, the mixture was transferred into a 30-mL Teflon-lined autoclave, followed by heating at 150 °C for 2 h. The final product was diluted 2000-fold in Tris-HCl buffer (50 mM, pH = 7.4) and was stored at 4 °C for further use.

Detection of D-pen and Cu^{2+}

Ten microliters of OPD (100 mM), 10 μL of Cu^{2+} (1 mM) and 10 μL of diluted sample or D-pen standard solution at various concentrations were successively introduced into 940 μL of Tris-HCl buffer (50 mM, pH = 7.4). The resulting solution was incubated at 37 °C for 3 h. Then, 30 μL

of CDs was added to the above solution. After subsequent incubation for 2 min at room temperature, the solution was examined by both ratiometric fluorescence and colorimetric modes. The ratio of fluorescence intensity at 443 nm against that at 555 nm (F_{443}/F_{555}) and the absorbance at 420 nm (A_{420}) were respectively recorded as the response signals of the above detection modes for detecting D-pen.

A description of the procedure for detecting Cu^{2+} is provided in the supporting information (SI) document.

Cytotoxicity assay and cell imaging

A549 lung cancer cells used for cytotoxicity assay and fluorescence imaging were cultured in Dulbecco's modified Eagle's medium (DMEM) with 10% fetal bovine serum albumin (BSA) under conditions of 37 °C, 95% relative humidity and 5% CO_2.

The cytotoxicity of CDs was evaluated by standard MTT assay (colorimetric procedure). A549 lung cancer cells were treated with various volumes of CDs in individual wells of an incubation dish, and the dish was then incubated at 37 °C for 24 h. Then, 20 μL of MTT solution in DMEM was added into each well after the removal of the culture medium. After another incubation for 4 h, 150 μL of dimethyl sulfoxide (DMSO) was added into each well, followed by gentle shaking for 10 min. Finally, the absorbance of each well was recorded at 378 nm with a microplate reader.

A549 lung cancer cells were successively treated with 10 μL of Cu^{2+} (1 mM) and different volumes of D-pen (1 mM) followed by incubation at 37 °C for 12 h. After washing with Tris-HCl buffer (50 mM, pH = 7.4), the cells were further treated with 30 μL of CDs and 10 μL of OPD (100 mM), and were then incubated at 37 °C for 3 h. Finally, the cells were washed with Tris-HCl buffer (50 mM, pH = 7.4) for fluorescence imaging on a confocal microscope.

Results and discussion

Characterizations of CDs

As displayed in the TEM image in Fig. 1a, the CDs are spherical and exhibit good dispersibility. The diameter of the CDs varied between 1.0 nm and 3.1 nm, with an average value of 2 nm (inset of Fig. 1a).

Identification of surface chemical groups and elemental analysis of CDs were performed by FT-IR (Fig. 1b) and XPS (Fig. 2) spectroscopy. In the FT-IR spectrum, the broad absorption band at 3426 cm^{-1} is associated with O–H or N–H stretching vibrations, the bands at 1654 cm^{-1} and 1617 cm^{-1} correspond to the stretching vibrations of C=O and C=N groups, respectively, the bands at 1560 cm^{-1} and 1383 cm^{-1} are assigned to the bending vibrations of N–H and C–N, and the band at 2916 cm^{-1} is attributed to C–H stretching vibration [37, 38]. The XPS spectra (Fig. 2) further reveal the elemental composition of the CDs. Three main peaks that emerged at 284.3 eV, 399.5 eV and 532.1 eV in the full-scan survey spectrum (Fig. 2a) correspond to C 1s (68.4%), N 1s (7.97%) and O 1s (23.63%), respectively [39]. In the high-resolution spectra of C 1s (Fig. 2b), four peaks appeared at 284.6 eV, 285.0 eV, 286.2 eV and 287.9 eV, which are derived from the C–C/C=C, C–N, C–O and C=N/C=O groups, respectively [40]. The two peaks at 399.8 and

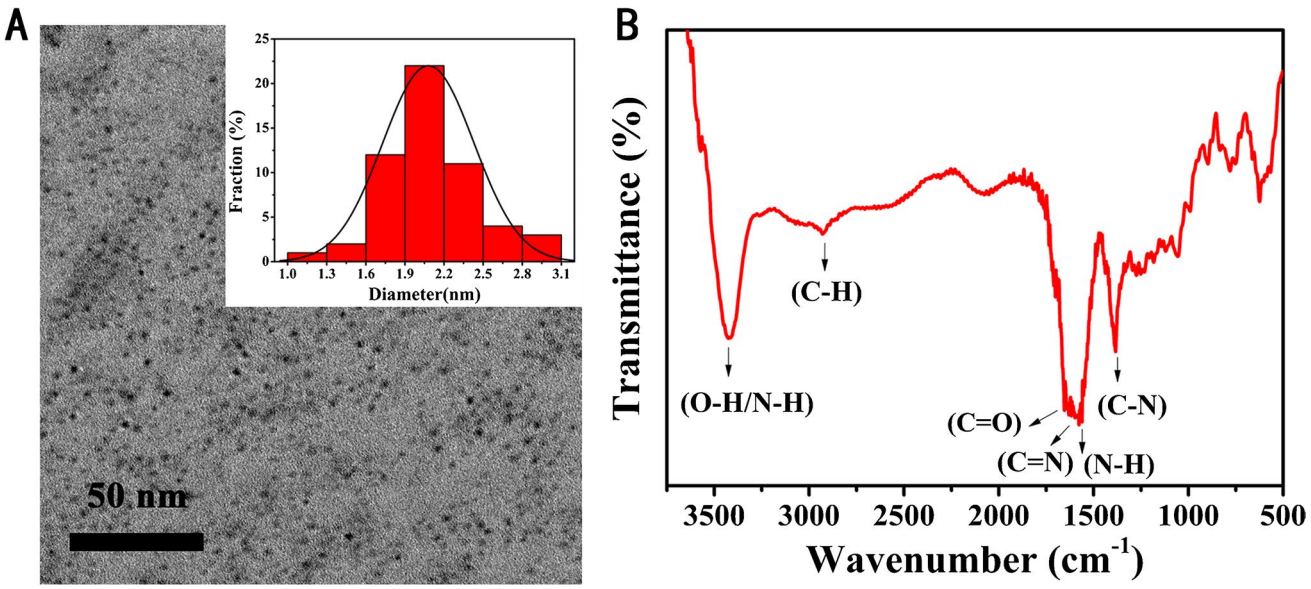

Fig. 1 **a** TEM image and particle size distribution of CDs. **b** FT-IR spectrum of CDs

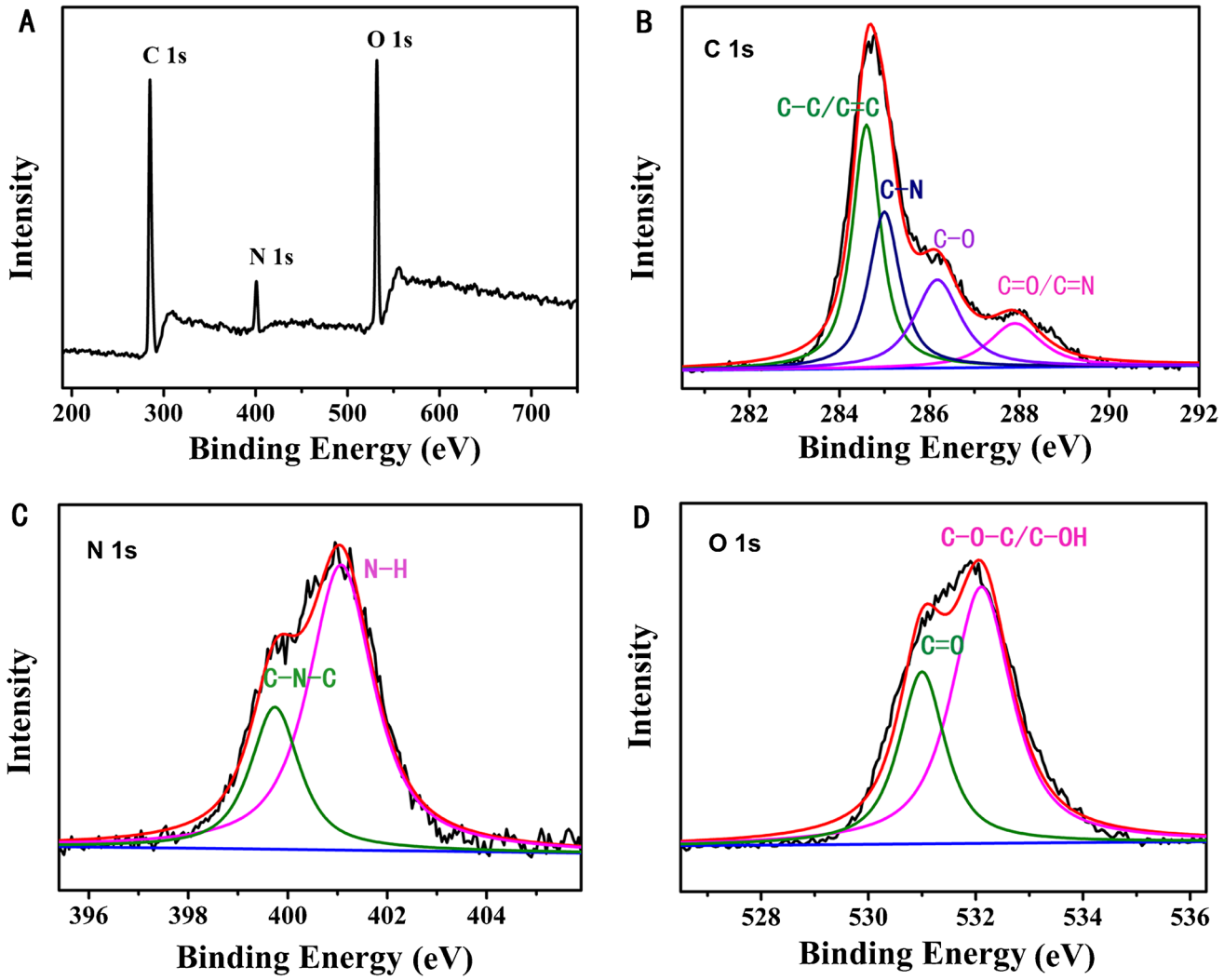

Fig. 2 **a** XPS full-scan survey spectrum of CDs. **b–d** High-resolution XPS spectra of C 1s, O 1s and N 1s, respectively

401.0 eV in the high-resolution spectrum of N 1s (Fig. 2c) can be ascribed to C–N–C and N–H [41]. There are two contributions of O demonstrated in the high-resolution spectrum of O 1s (Fig. 2d), corresponding to 531.5 eV for C=O and 532.1 eV for C–O–C/C–OH. The results of the XPS analysis are consistent with those obtained by FT-IR measurement.

Optical properties of CDs

The optical properties of the CDs were studied by UV-Vis absorption and fluorescence spectroscopy. As displayed in Fig. 3a, two obvious absorption bands emerged at 240 nm and 350 nm (dotted line), which correspond to the π–π* transitions of the alkene group or carbonyl group (C=C/C=O) and the π–π* transitions of the amine moiety [42, 43]. Two excitation peaks at 242 and 352 nm indicate that there are at least two types of excitation energy trapped on the CDs (red line), which is consistent with information revealed by the above UV-Vis absorption spectrum. Figure 3b shows the fluorescence emission spectra of the CDs at different excitation wavelengths between 300 nm and 380 nm, demonstrating a very slight excitation-dependent shift. The fluorescence quantum yield (QY) of the CDs was evaluated using quinine sulfate (QY = 54.60% in 0.1 M H_2SO_4 solution) as the standard reference. A relatively high QY (27.08%) of the CDs suggests their potential for applications in fluorescence imaging and detection systems; the concrete calculation formula is in the supporting information (SI) document.

Fluorescence emission stability of CDs

The effects of environmental pH and ionic strength on the fluorescence emission stability of the CDs were explored. As depicted in Fig. S1a, the fluorescence emission of the CDs was slightly influenced by the environmental pH levels varying from 4.0 to 8.0. Figure S1b shows that the fluorescence

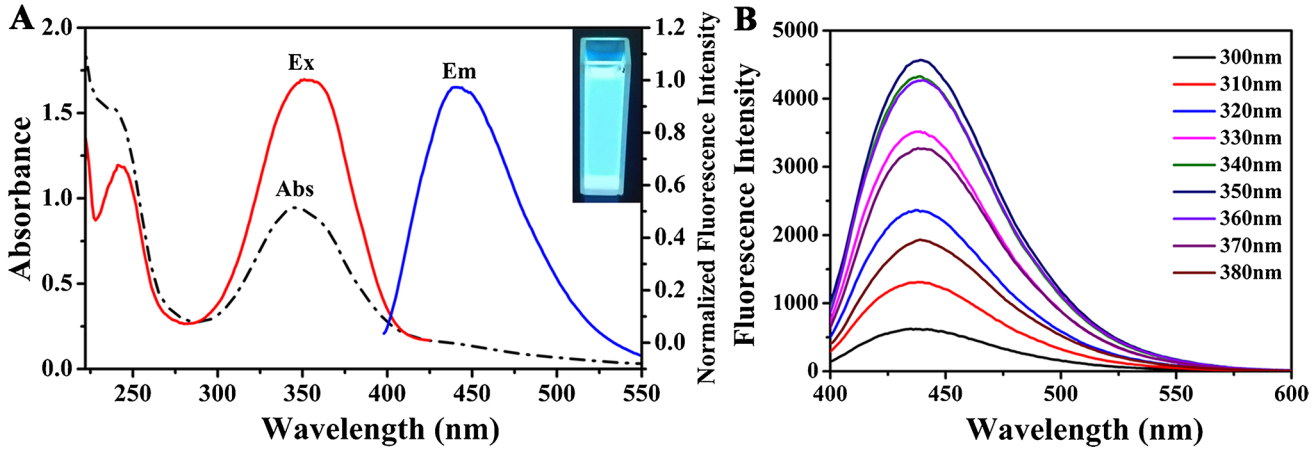

Fig. 3 **a** UV-Vis absorption (Abs), fluorescence excitation (Ex) and emission (Em) spectra of CDs. The inset photograph shows the color of CDs under UV (365 nm) light. **b** Fluorescence emission spectra of CDs at different excitation wavelengths

intensity of the CDs exhibits no obvious change under high ionic strength (NaCl, 5 M). The results of photobleaching experiments (Fig. S1c) reveal the good photobleaching resistance of the CDs under ultraviolet irradiation at 378 nm for 60 min. These results indicate that the synthesized CDs have sufficient fluorescence emission stability for further chemical or biological applications.

Optimization of experimental parameters

In order to obtain superior analytical performance, the effects of experimental conditions including environmental pH and incubation time were investigated. According to the results shown in Fig. S2a, Tris-HCl buffer (50 mM, pH = 7.4) was selected to maintain the environmental pH level for the following experiments, since the normal pH of human blood pH is 7.4. The incubation time of this sensing platform prior to analysis was also optimized, and the results (Fig. S2b) suggest that an incubation time of 3 h is sufficient for oxidation and chelation reactions. The excitation wavelength of this sensing platform was set at 378 nm to both ensure the fluorescence emission efficiencies and obtain comparable fluorescence intensities of CDs and oxOPD at 443 nm and 555 nm (Fig. S2c), respectively.

Sensing mechanism

The response mechanism of this sensing platform was studied by fluorescence emission spectroscopy (Fig. 4a), UV-Vis absorption spectroscopy (Fig. 4b) and fluorescence decay profile (Fig. 4c). As shown in Fig. 4a, the fluorescence emission of the CDs at 443 nm was influenced very slightly by individually adding Cu^{2+} or OPD to the testing system. After adding both Cu^{2+} and OPD to the testing system, however, the fluorescence at 443 nm decreased significantly, and a new fluorescence emission peak at 555 nm emerged. These results were ascribed to the generation of oxOPD, a product of the specific oxidation of OPD by Cu^{2+}. Additionally, oxOPD induced an obvious absorption band at 420 nm (Fig. 4b). D-pen itself exhibited little fluorescence emission, but it inhibited the oxidation of OPD by chelating with the oxidant Cu^{2+}, which obviously restricted the absorption band of oxOPD at 420 nm (Fig. 4b) and, consequently, facilitated the fluorescence emission of the CDs at 443 nm (Fig. 4a). Therefore, the intensity ratio of fluorescence emission at 443 nm against that at 555 nm (F_{443}/F_{555}) and the absorbance at 420 nm (A_{420}) are suitable for indicating the amount of D-pen in the testing system.

It can be observed that the absorption spectrum of oxOPD overlaps with the fluorescence emission spectrum of the CDs (Fig. 4d). Moreover, the fluorescence lifetime of the CDs decreased after introducing Cu^{2+} and OPD into the testing system (Fig. 4c). These results suggest the strong possibility of a FRET process during the fluorescence quenching of CDs at 443 nm in the testing system containing Cu^{2+} and OPD. Therefore, the Forster distance (R_0) between the donor (CDs) and the acceptor (oxOPD) at which the FRET efficiency equals 50% was estimated according to equations provided in literature. [[44]]

$$R_0^6 = 8.79 \times 10^{-25} k^2 n^{-4} \Phi J$$

$$J = \frac{\sum F(\lambda)\, \varepsilon(\lambda)\, \lambda^4\, \Delta\lambda}{\sum F(\lambda)\, \Delta(\lambda)}$$

where k^2 refers to the statistically relative orientation of the transition dipoles of donors and acceptors in space (in fluid solution $k^2 = 2/3$ for random orientation); n is the refractive index of medium (in this work $n = 1.33$); Φ is the fluorescence quantum yield of the CDs synthesized in this work

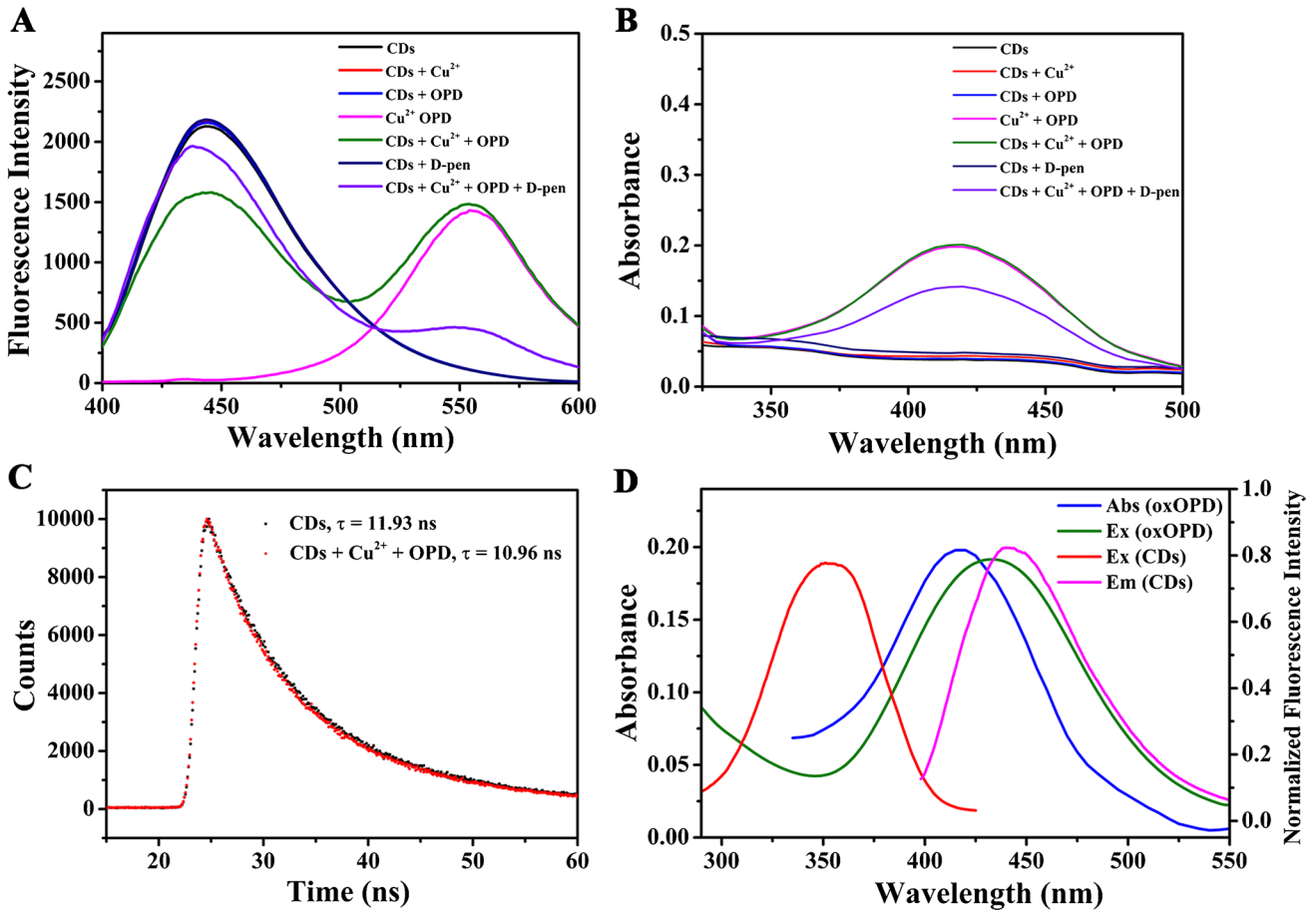

Fig. 4 Spectra of **a** fluorescence emission and **b** UV-Vis absorption of the testing system. **c** Fluorescence emission decay curves of CDs in the absence and presence of Cu^{2+} and OPD. **d** Typical spectra of absorption of oxOPD, fluorescence excitation of oxOPD and CDs, fluorescence emission of CDs. The excitation wavelength for scanning fluorescence emission spectra was 378 nm. The excitation and emission wavelengths for fluorescence decay testing were 360 nm and 450 nm, respectively. Concentrations of testing reagents were as follows: Cu^{2+}, 10 μM; OPD, 1 mM; D-pen, 400 μM in (**a**) and 100 μM in (**b**)

(27.08%); *J* refers to the overlap spectral integral between the fluorescence emission of the CDs and the extinction coefficients of oxOPD within a wavelength range in which the emission and absorption spectra overlap efficiently (in this work a wavelength range of 400–500 nm was selected); *ε(λ)* is the molar absorption coefficient of oxOPD (the maximum value is 2.1×10^4 L mol^{-1} cm^{-1} at 440 nm [45]) at a certain wavelength λ in the above wavelength range. The final calculated values of *J* and R_0 for this work are 6.2×10^{-14} cm^3 L mol^{-1} and 3.8 nm, respectively, indicating the close proximity of donor and acceptor for efficient transfer of fluorescence resonance energy. The electrostatic interaction between deprotonated carboxyl groups on the surface of thr CDs and protonated amino groups of oxOPD molecules, and the π–π stacking interaction between the CDs and oxOPD molecules may contribute to the formation of the FRET system. The difference between the FT-IR spectra (Fig. S3) of the testing systems containing various amount of CDs, reactants (Cu^{2+} and OPD) and inhibitor (D-pen) of the oxidation reaction reveals that oxOPD is the product of this reaction, while D-pen efficiently inhibits this reaction. Based on the above discussion, FRET between the CDs and oxOPD was confirmed as one of the fluorescence quenching mechanisms of this sensing platform.

Moreover, the obvious overlap between the fluorescence excitation spectrum of thr CDs and the spectral absorption of oxOPD reveals their competitive nature. This competition leads to the typical primary inner filter effect (pIFE or IFE1) [46] of oxOPD on the fluorescence emission of CDs.

Selectivity

To evaluate the selectivity of the present sensing platform towards D-pen, the influence of common ions and biological substances coexisting in human serum or urine on the detection results was investigated. The results illustrated in Fig. S4 reveal that no obvious interference from the above ions or substances was observed, indicating the good

selectivity of the sensing platform. It is worth noting that OPD can also be oxidized by Ag^+, since the oxidizing activity of Ag^+ is greater than that of Cu^{2+}. However, Cl^- ions in Tris-HCl buffer react with Ag^+ to form precipitated AgCl, which efficiently removes Ag^+ from the testing system.

Analytical performance

Figure 5 demonstrates the fluorescence and UV-Vis responses of the sensing platform towards D-pen. With the increasing concentration of D-pen, the color of the testing system changes gradually from yellow to blue under the illumination of a 365-nm UV lamp (inset of Fig. 5a), and from yellow to colorless under daylight (inset of Fig. 5c). As shown in Fig. 5b, a good linear relationship was found between the fluorescence ratio F_{443}/F_{555} and the D-pen concentration ranging from 0.5 μM to 50.0 μM. The limit of detection (LOD) for D-pen obtained by the fluorescence testing mode was calculated as 0.092 μM ($S/N = 3$). The absorbance at 420 nm (A_{420}) also correlates linearly with the D-pen concentration in the range of 0.9–40.0 μM (Fig. 5d). The LOD for D-pen obtained by the UV-Vis absorption mode is 0.848 μM. These results indicate that the sensitivity of this sensing platform for D-pen detection is comparable to or slightly better than many reported methods (Table 1).

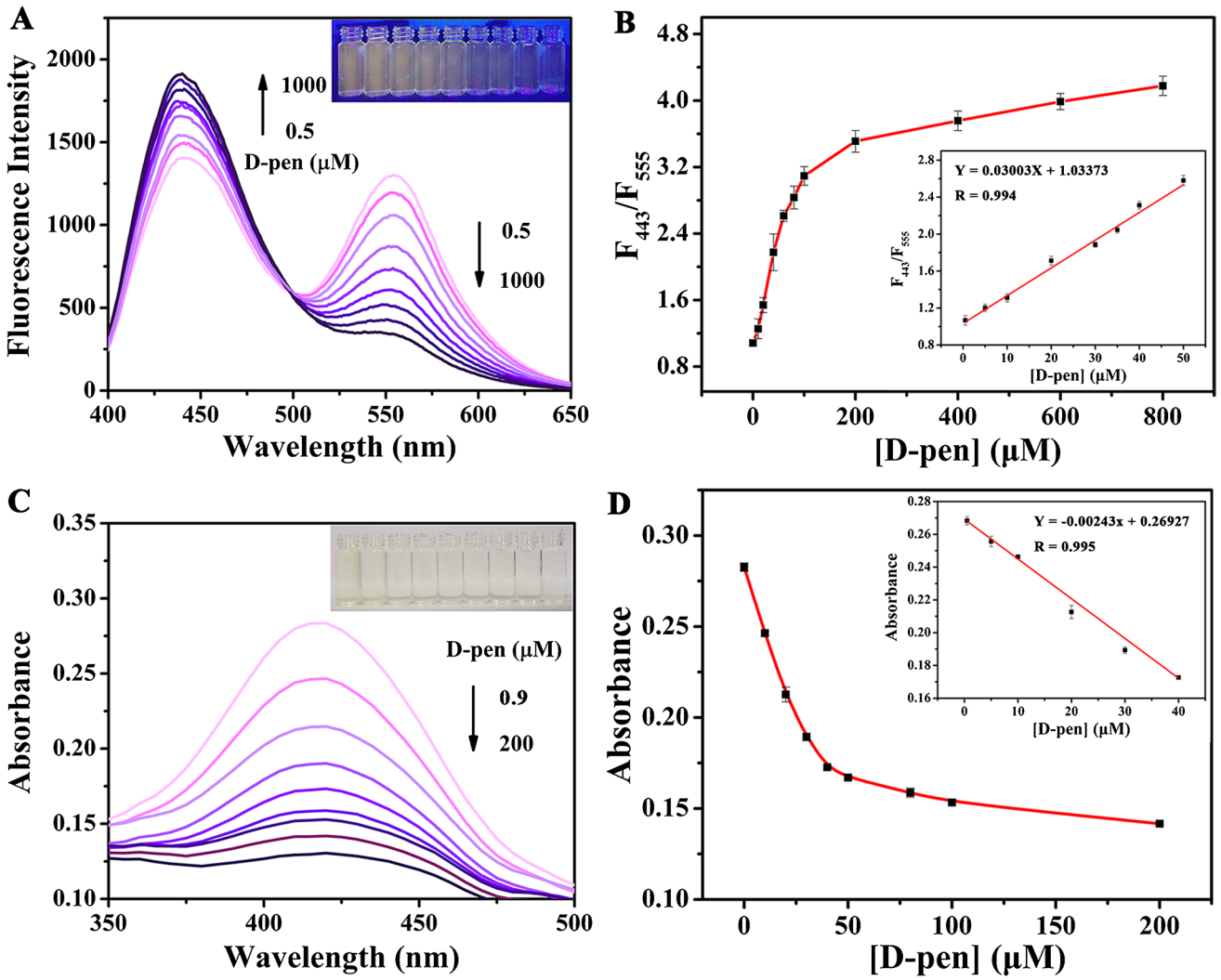

Fig. 5 **a** Fluorescence spectra of the sensing system with different D-pen concentrations (0.5, 10, 15, 30, 50, 80, 200, 800, and 1000 μM). The inset photographs show the corresponding color changes under UV light. **b** Plot of fluorescence responses against concentrations of D-pen. **c** UV-Vis absorption spectra of the sensing system with different D-pen concentrations (0.9, 10, 30, 35, 40, 80, 100, 180, and 200 μM). The inset photographs show the corresponding color changes under daylight. **d** Plot of absorbance against concentration of D-pen

Table 1 Comparison of analytical performance of the present sensing platform and reported methods for detecting D-pen

Methods	Chemosensor	Linear range (μM)	LOD (μM)	Reference
Electrochemistry	$Ni_3S_4/NiS_2/MoO_x$/GC electrode[a]	5.0–796.0	0.26	[20]
Electrochemistry	MIP-GCE[b]	10.0–480.0	3.5	[47]
Liquid chromatography	CMQT-derivatization[c]	1.0–200.0	Not given	[48]
Infrared spectroscopy	VPG-FTIR[d]	26.8–2546.0	3.4	[21]
Fluorometry	AuNCs[e]	20.0–239.0	5.4	[49]
Fluorometry	CdS QDs[f]	0.67–5.36	0.75	[50]
Ratiometric Fluorometry	CDs[g]	0.5–50.0	0.092	This work
Colorimetry	CDs	0.9–40.0	0.848	This work

[a]$Ni_3S_4/NiS_2/MoO_x$/GC electrode: $Ni_3S_4/NiS_2/MoO_x$ composite-coated glassy carbon electrode;

[b]MIP-GCE: molecularly imprinted polypyrrole-modified glassy carbon electrode; [c]CMQT-derivatization: 2-chloro-1-methylquinolinium tetrafluoroborate derivatization; [d]VPG-FTIR: online system with vapor phase generation and Fourier transform infrared (FTIR) spectrometry;

[e]AuNCs: gold nanoclusters;

[f]CdS QDs: CdS quantum dots;

[g]CDs: carbon dots

Detection of D-pen in real body fluid samples

To estimate the practicability of the present sensing platform, it was applied to examine the spiked real samples by both ratiometric fluorescence and colorimetric (UV-Vis absorption) modes. All the blank and spiked samples were verified by an HPLC method recommended in the United States Pharmacopeia, 2008. The human serum and urine samples were diluted 100-fold prior to testing. Results listed in Table 2 show that the recoveries for all testing modes and sample types were limited in the range of 98.2–102.6%, which demonstrates the promising potential of the present sensing platform for the determination of D-pen in real samples.

Cytotoxicity and cell imaging

The overall cellular cytotoxicity of the reagents employed or generated in the sensing platform is dominant for biological applications. Results obtained by the MTT assays (Fig. S7) show that the viability of A549 lung cancer cells was higher than 75% after treatment with CDs, Cu^{2+} and OPD, indicating the low cell toxicity of these testing reagents.

Fluorescence images of cells treated with Cu^{2+} or D-pen and other testing reagents are shown in Fig. 6. The corresponding fluorescence variations of purple and green channels of these images, and the relationship between the fluorescence intensity ratios of the above channels and concentrations of D-pen, are illustrated in Fig. S8. It can be observed that the fluorescence intensity of the green

Table 2 Results for D-pen detection in human serum and urine samples ($n = 3$)

Samples	Testing mode	Spiked (μM)	Found (μM)	Recovery (%)	RSD (%)
Serum	Ratiometric fluorometry	10.0	10.08	100.8	0.56
		20.0	20.23	101.1	1.15
		40.0	39.82	99.6	0.15
	Colorimetry	10.0	9.88	98.8	0.68
		20.0	20.51	102.6	1.29
		40.0	39.28	98.2	2.31
Urine	Ratiometric fluorometry	10.0	10.17	101.7	0.91
		20.0	20.48	102.4	1.28
		40.0	39.82	99.6	0.35
	Colorimetry	10.0	10.11	101.1	0.58
		20.0	20.07	100.4	0.32
		40.0	39.41	98.5	1.41

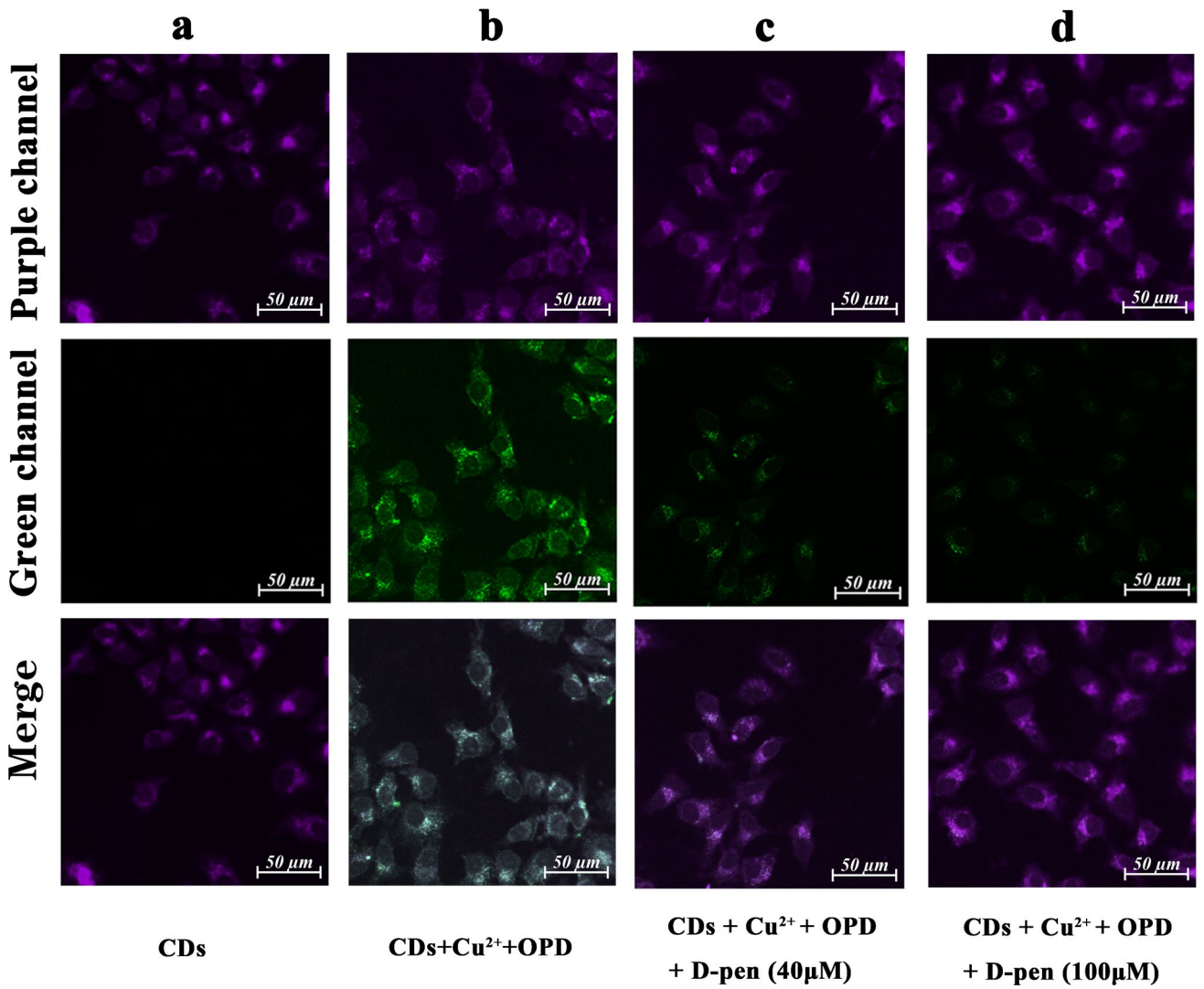

Fig. 6 Fluorescence images of live A549 lung cancer cells. **a** Cells treated with CDs; **b** cells treated successively with Cu^{2+}, CDs and OPD; **c**–**d** cells treated successively with Cu^{2+}, D-pen, CDs and OPD. The excitation wavelength was set as 378 nm. The wavelength ranges of the purple channel and green channel were 400–500 nm and 500–600 nm, respectively. The amount of CDs was 30 μL. Concentrations of Cu^{2+} and OPD were 10 μM and1 mM, respectively

channel decreased with the increase in D-pen concentration in the testing system, while the purple channel exhibited an opposite trend. These results reveal that the testing reagents used in the present sensing platform possess good cell membrane permeability, which makes the fluorescence analysis of D-pen in cells possible.

Conclusion

In summary, we fabricated a ratiometric fluorescence and colorimetric dual-mode sensing platform based on CDs and OPD for highly sensitive determination of Cu^{2+} and D-pen. The facilely synthesized CDs displayed excellent optical properties and good fluorescence emission stability. During the analytical procedure, OPD was oxidized by Cu^{2+} to generate fluorescent oxOPD, which induced absorbance at 420 nm, fluorescence emission at 555 nm, and quenching of fluorescence emitted from CDs at 443 nm via IFE and FRET. Importantly, D-pen inhibited the above oxidation reaction because of its strong chelation affinity towards Cu^{2+}. Therefore, the amount of Cu^{2+} and D-pen in the testing system correlated with the intensity ratio of fluorescence emission at 443 nm to that at 555 nm (F_{443}/F_{555}), as well as the absorbance at 420 nm (A_{420}). The proposed sensing platform exhibits high reliability, selectivity and sensitivity for determination of D-pen in human serum and urine samples, demonstrating its promising potential for future applications in the study of pharmacodynamics and clinical diagnosis.

Supplementary Information The online version contains supplementary material available at https://doi.org/10.1007/s00216-021-03789-4.

Acknowledgements This work was supported by the Science and Technology Development Plan of Jilin Province (No. 202002056JC), the Industrialization Project of the Education Department of Jilin Province (No. JJKH20200944KJ), the National Natural Science Foundation of China (No. 82004005), the Fundamental Research Funds for the Central Universities of China, and the Training Program of Excellent Young Teachers of Jilin University.

Author contributions All authors have given approval for the final version of the paper.

Declarations

All applicable international, national, and/or institutional guidelines for the collection and use of human blood and serum samples were followed.

Declaration of competing interests The authors declare that they have no known competing financial interests or personal relationships that could have appeared to influence the work reported in this paper.

Human ethics The study was approved by the Institutional Ethics Committee of China-Japan Union Hospital of Jilin University, Changchun, China (No. 2019040811).

References

1. Bieri M. D-Penicillamine adsorption on gold: an in situ ATR-IR spectroscopic and QCM study. Langmuir. 2006;22:8379–86.
2. Kim HA, Song YW. A comparison between bucillamine and D-penicillamine in the treatment of rheumatoid arthritis. Rheumatol Int. 1997;17:5–9.
3. Preedy VR, Wassif WS, Baldwin D, Jones J, Falkous G, Marway JS, Mantle D, Scott DL. Skeletal muscle protein loss due to D-penicillamine results from reduced protein synthesis. Int J Biochem Cell B. 2001;33(10):1013–26.
4. Cope-Yokoyama S, Finegold MJ, Sturniolo GC, Kim K, Mescoli C, Rugge M, Medici V. Wilson disease: histopathological correlations with treatment on follow-up liver biopsies. World J Gastroenterol. 2010;16(12):1487–94.
5. Joly D, Rieu P, Mejean A, Gagnadoux MF, Daudon M, Jungers P. Treatment of cystinuria. Pediatr Nephrol. 1999;13(9):945–50.
6. Dodani SC, Firl A, Chan J, Nam CI, Aron AT, Onak CS, Ramos-Torres KM, Paek J, Webster CM, Feller MB, Chang CJ. Copper is an endogenous modulator of neural circuit spontaneous activity. Proc Natl Acad Sci U S A. 2014;111(46):16280–5.
7. Chen J, Jiang Y, Shi H, Peng Y, Fan X, Li C. The molecular mechanisms of copper metabolism and its roles in human diseases. Pflugers Arch. 2020;472(10):1415–29.
8. Uriu-Adams JY, Keen CL. Copper, oxidative stress, and human health. Mol Asp Med. 2005;26(4-5):268–98.
9. Sarkar B. Treatment of Wilson and Menkes diseases. Chem Rev. 1999;99:2535–44.
10. Xu X, Ray R, Gu Y, Ploehn HJ, Gearheart L, Raker K, Scrivens WA. Electrophoretic analysis and purification of fluorescent single-walled carbon nanotube fragments. J Am Chem Soc. 2004;126(40):12736–7.
11. Sun YP, Zhou B, Lin Y, Wang W, Fernando KA, Pathak P, Meziani MJ, Harruff BA, Wang X, Wang H, Luo PG, Yang H, Kose ME, Chen B, Veca LM, Xie SY. Quantum-sized carbon dots for bright and colorful photoluminescence. J Am Chem Soc. 2006;128(24):7756–7.
12. Yang ST, Cao L, Luo PG, Lu F, Wang X, Wang H, Meziani MJ, Liu Y, Qi G, Sun YP. Carbon dots for optical imaging in vivo. J Am Chem Soc. 2009;131(32):11308–9.
13. Peng H, Zhang L, Kjallman TH, Soeller C, Travas-Sejdic J. DNA hybridization detection with blue luminescent quantum dots and dye-labeled single-stranded DNA. J Am Chem Soc. 2007;129(11):3048–9.
14. Weng CI, Chang HT, Lin CH, Shen YW, Unnikrishnan B, Li YJ, Huang CC. One-step synthesis of biofunctional carbon quantum dots for bacterial labeling. Biosens Bioelectron. 2015;68:1–6.
15. Chen BB, Liu ML, Zhan L, Li CM, Huang CZ. Terbium(III) modified fluorescent carbon dots for highly selective and sensitive ratiometry of stringent. Anal Chem. 2018;90(6):4003–9.
16. Wei Z, Li H, Liu S, Wang W, Chen H, Xiao L, Ren C, Chen X. Carbon dots as fluorescent/colorimetric probes for real-time detection of hypochlorite and ascorbic acid in cells and body fluid. Anal Chem. 2019;91(24):15477–83.
17. Zhang ZD, Baeyens WRG, Zhang XR, Weken GVD. Chemi luminescence determination of penicillamine via flow injection applying a quinine-cerium(iv) system. Analyst. 1996;121:1569.
18. Yuan Y, Zhao X, Liu S, Li Y, Shi Y, Yan J, Hu X. A fluorescence switch sensor used for D-Penicillamine sensing and logic gate based on the fluorescence recovery of carbon dots. Sensors Actuators B Chem. 2016;236:565–73.
19. Rojanarata T, Opanasopit P, Ngawhirunpat T, Saehuan C. Ninhydrin reaction on thiol-reactive solid and its potential for the quantitation of D-penicillamine. Talanta. 2010;82(2):444–9.
20. Kumar DR, Baynosa ML, Dhakal G, Shim JJ. Sphere-like Ni_3S_4/NiS_2/MoO_x composite modified glassy carbon electrode for the electrocatalytic determination of D-penicillamine. J Mol Liq. 2020;301:112447.
21. Zeeb M, Ganjali MR, Norouzi P, Moeinossadat SR. Selective determination of penicillamine by on-line vapor-phase generation combined with Fourier transform infrared spectrometry. Talanta. 2009;78(2):584–9.
22. Keating LR, LaCourse WR. Indirect pulsed electrochemical detection following high-performance reversed-phase liquid chromatography. Talanta. 2019;199:155–63.
23. Xu S, Zhang F, Xu L, Liu X, Ma P, Sun Y, Wang X, Song D. A fluorescence resonance energy transfer biosensor based on carbon dots and gold nanoparticles for the detection of trypsin. Sensors Actuators B Chem. 2018;273:1015–21.
24. Liu Y, Zhang Y, Zhang X, Zhang W, Wang X, Sun Y, Ma P, Huang Y, Song D. Near-infrared fluorescent probe based on ag&Mn:ZnInS QDs for tyrosinase activity detection and inhibitor screening. Sensors Actuators B Chem. 2021;344:130234.
25. Becker JS, Matusch A, Depboylu C, Dobrowolska J, Zoriy MV. Quantitative imaging of selenium, copper, and zinc in thin sections of biological tissues (slugs-genus Arion) measured by laser ablation inductively coupled plasma mass spectrometry. Anal Chem. 2007;79:6074–80.
26. Ndokoye P, Ke J, Liu J, Zhao Q, Li X. L-cysteine-modified gold nanostars for SERS-based copper ions detection in aqueous media. Langmuir. 2014;30(44):13491–7.
27. Ozkantar N, Yilmaz E, Soylak M, Tuzen M. Pyrocatechol violet impregnated magnetic graphene oxide for magnetic solid phase microextraction of copper in water, black tea and diet supplements. Food Chem. 2020;321:126737.
28. Zaksas NP, Gerasimov VA, Nevinsky GA. Simultaneous determination of Fe, P, Ca, Mg, Zn, and Cu in whole blood by two-jet plasma atomic emission spectrometry. Talanta. 2010;80(5):2187–90.

29. Xu Z, Meng Q, Cao Q, Xiao Y, Liu H, Han G, Wei S, Yan J, Wu L. Selective sensing of copper ions by mesoporous porphyrinic metal-organic framework nanoovals. Anal Chem. 2020;92(2):2201–6.
30. Dong Y, Wang R, Li G, Chen C, Chi Y, Chen G. Polyamine-functionalized carbon quantum dots as fluorescent probes for selective and sensitive detection of copper ions. Anal Chem. 2012;84(14):6220–4.
31. Li J, Mo F, Guo L, Huang J, Lu Z, Xu Q, Li H. Ligand reduction and cation exchange on nanostructures for an elegant design of copper ions photoelectrochemical sensing. Sensors Actuators B Chem. 2021;328:129032.
32. Jin LH, Han CS. Ultrasensitive and selective fluorimetric detection of copper ions using thiosulfate-involved quantum dots. Anal Chem. 2014;86(15):7209–13.
33. Lu W, Gao Y, Jiao Y, Shuang S, Li C, Dong C. Carbon nano-dots as a fluorescent and colorimetric dual-readout probe for the detection of arginine and Cu^{2+} and its logic gate operation. Nanoscale. 2017;9(32):11545–52.
34. Khan IM, Niazi S, Yu Y, Mohsin A, Mushtaq BS, Iqbal MW, Rehman A, Akhtar W, Wang Z. Aptamer induced multicolored AuNCs-WS_2 "turn on" FRET nano platform for dual-color simultaneous detection of AflatoxinB1 and Zearalenone. Anal Chem. 2019;91(21):14085–92.
35. Deng L, Liu Q, Lei C, Zhang Y, Huang Y, Nie Z, Yao S. Fluorometric and colorimetric dual-readout assay for histone demethylase activity based on formaldehyde inhibition of ag^{+}-triggered oxidation of O-Phenylenediamine. Anal Chem. 2020;92(13):9421–8.
36. Fang H, Yu H, Lu Q, Fang X, Zhang Q, Zhang J, Zhu L, Ma Q. A new ratiometric fluorescent probe for specific monitoring of hROS under physiological conditions using boric acid-protected L-DOPA gold nanoclusters. Anal Chem. 2020;92(19):12825–32.
37. Liu S, Cui J, Huang J, Tian B, Jia F, Wang Z. Facile one-pot synthesis of highly fluorescent nitrogen-doped carbon dots by mild hydrothermal method and their applications in detection of Cr(VI) ions. Spectrochim Acta A. 2019;206:65–71.
38. Han Z, Nan D, Yang H, Sun Q, Pan S, Liu H, Hu X. Carbon quantum dots based ratiometric fluorescence probe for sensitive and selective detection of Cu^{2+} and glutathione. Sensors Actuators B Chem. 2019;298:126842.
39. Liu S, Tian J, Wang L, Zhang Y, Qin X, Luo Y, Asiri AM, Al-Youbi AO, Sun X. Hydrothermal treatment of grass: a low-cost, green route to nitrogen-doped, carbon-rich, photoluminescent polymer nanodots as an effective fluorescent sensing platform for label-free detection of Cu(II) ions. Adv Mater. 2012;24(15):2037–41.
40. Zou XX, Li GD, Wang YN, Zhao J, Yan C, Guo MY, Li L, Chen JS. Direct conversion of urea into graphitic carbon nitride over mesoporous TiO_2 spheres under mild condition. Chem Commun. 2011;47(3):1066–8.
41. Liu S, Tian J, Wang L, Luo Y, Zhai J, Sun X. Preparation of photoluminescent carbon nitride dots from CCl_4 and 1,2-ethylenediamine: a heat-treatment-based strategy. J Mater Chem. 2011;21:11726.
42. Gu D, Shang S, Yu Q, Shen J. Green synthesis of nitrogen-doped carbon dots from lotus root for Hg(II) ions detection and cell imaging. Appl Surf Sci. 2016;390:38–42.
43. Atchudan R, Edison TNJI, Chakradhar D, Perumal S, Shim J-J, Lee YR. Facile green synthesis of nitrogen-doped carbon dots using Chionanthus retusus fruit extract and investigation of their suitability for metal ion sensing and biological applications. Sensors Actuators B Chem. 2017;246:497–509.
44. Yuan Y, Jiang J, Liu S, Yang J, Zhang H, Yan J, Hu X. (2017) Fluorescent carbon dots for glyphosate determination based on fluorescence resonance energy transfer and logic gate operation. Sensors Actuators B Chem. 2017;242:545-553.
45. Mekler VM, Bystryak SM. Autosensitized oxidation of *o*-phenylenediamine in an queueous buffer solution. J Photoch Photobio A. 1992;65(15):391–7.
46. Chen S, Yu YL, Wang JH. Inner filter effect-based fluorescent sensing systems: a review. Anal Chim Acta. 2018;999:13–26.
47. Li BL, Luo JH, Luo HQ, Li NB. A novel strategy for selective determination of D-penicillamine based on molecularly imprinted polypyrrole electrode via the electrochemical oxidation with ferrocyanide. Sensors Actuators B Chem. 2013;186:96–102.
48. Kusmierek K, Bald E. Simultaneous determination of tiopronin and D-penicillamine in human urine by liquid chromatography with ultraviolet detection. Anal Chim Acta. 2007;590(1):132–7.
49. Wang P, Li BL, Li NB, Luo HQ. A fluorescence detection of D-penicillamine based on Cu^{2+}-induced fluorescence quenching system of protein-stabilized gold nanoclusters. Spectrochim Acta A. 2015;135:198–202.
50. Pawar SP, Gore AH, Walekar LS, Anbhule PV, Patil SR, Kolekar GB. Turn-on fluorescence probe for selective and sensitive detection of D-penicillamine by CdS quantum dots in aqueous media: application to pharmaceutical formulation. Sensors Actuators B Chem. 2015;209:911–8.